

# An effective model of magnetoelectricity in multiferroics $\text{RMn}_2\text{O}_5$

CHEN FANG and JIANGPING HU<sup>(a)</sup>

*Department of Physics, Purdue University - West Lafayette, IN 47907, USA*

received 15 January 2008; accepted in final form 8 April 2008

published online 26 May 2008

PACS 75.25.+z – Spin arrangements in magnetically ordered materials (including neutron and spin-polarized electron studies, synchrotron-source X-ray scattering, etc.)

PACS 75.47.Lx – Manganites

PACS 77.80.-e – Ferroelectricity and antiferroelectricity

**Abstract** – An effective model is developed to explain the phase diagram and the mechanism of magnetoelectric coupling in multiferroics,  $\text{RMn}_2\text{O}_5$ . We show that the nature of magnetoelectric coupling in  $\text{RMn}_2\text{O}_5$  is a coupling between two Ising-type orders, namely, the ferroelectric order in the  $b$ -axis, and the coupled magnetic order between two frustrated antiferromagnetic chains. The frustrated magnetic structure drives the system to a commensurate-incommensurate phase transition, which can be understood as a competition between a collinear order stemming from the “order by disorder” mechanism and a chiral symmetry order. The low-energy excitation is calculated and it quantitatively matches experimental results. Distinct features and the effects of external magnetic field in the electromagnon spectra in the incommensurate phase are predicted.

Copyright © EPLA, 2008

Recently, the search for new spin-electronics materials has led to the discovery of novel gigantic magnetoelectric and magnetocapacitive effects in rare-earth manganites, magnetoelectric multiferroics [1,2]. Unlike the magnetic ferroelectrics studied in the 1960s and 1970s where magnetism and ferroelectricity couple weakly, the magnetism and ferroelectricity in the new materials couple so strongly that the ferroelectricity can be easily manipulated by applying a magnetic field and the magnetic phase can be controlled by applying an electric field [3,4]. This ease of manipulation promises great potential for important technological applications in novel spintronics devices.

The physics of the multiferroics involves the interplay between many degrees of freedom, such as charge, spin, orbital and lattice. Tremendous effort has been devoted to decode the fundamental mechanism of the strong coupling between the magnetism and ferroelectricity. Experimentally, two major classes of magnesium oxide multiferroics, have been discovered. The first class is the orthorhombic rare-earth manganites  $\text{RMnO}_3$  ( $R = \text{Gd, Tb, Dy, } \dots$ ) [5,6], characterized by spiral magnetism strongly coupled with the ferroelectricity. An effective Ginzburg-Landau theory incorporating the space group symmetry and time-reversal symmetry has been constructed to explain the fundamental physics [7]. Microscopically, Dzyaloshinskii-Moriya

spin-orbit interaction is the underlying mechanism of the ferroelectricity [8–10] and an electric current cancellation principle related to spin-orbit coupling can also explain the physics [11]. The second class of materials are the manganese oxides with general formula  $\text{RMn}_2\text{O}_5$  ( $R = \text{Y, Tb, Dy, } \dots$ ) [12–15]. These insulating materials consist of linked  $\text{Mn}^{4+}\text{O}_6$  octahedra and  $\text{Mn}^{3+}\text{O}_5$  pyramids with a  $Pbam$  space group symmetry. Unlike that in  $\text{RMnO}_3$ , the ferroelectricity in  $\text{RMn}_2\text{O}_5$  exists in a collinear magnetic phase, suggesting that a different mechanism is involved in the interaction between the ferroelectricity and magnetism.

In this letter, we develop an effective model to explain the phase diagram and the mechanism of magnetoelectric coupling in  $\text{RMn}_2\text{O}_5$ . Building upon experimental facts and the space group symmetry [4,12–20], we show that the magnetoelectric interaction is between two Ising-type orders, the ferroelectric order in the  $b$ -axis and the coupled magnetic order between two frustrated antiferromagnetic chains. The effective model of the magnetism can be derived from a microscopic model with nearest-neighbor magnetic exchange. We show that the effective model nicely captures the phase diagrams of  $\text{RMn}_2\text{O}_5$ . At high temperature, the commensurate (CM) collinear order is stable due to the “order by disorder” mechanism [21–23] and the existence of an easy axis. As the temperature decreases, a chiral symmetry order replaces the collinear order, and the magnetic structure

<sup>(a)</sup>E-mail: hu4@purdue.edu

becomes incommensurate (ICM). This model predicts that an external magnetic field along the  $b$ -axis can drive the system from the ICM phase to the CM phase, while that along the  $a$ -axis can drive the system from the CM phase to the ICM phase. We also show that the model not only quantitatively explains the experimental results on the electromagnon spectra [20], but also predicts the following distinctive properties of low-energy excitations: 1) the emergence of electromagnons in the ICM phase when there is no electromagnons at the lowest energy in the CM phase; 2) the presence of distinguished kinks in the energy dispersions of the electromagnons, unlike the dispersion of normal phasons in conventional ICM phase which has a finite energy jump at the half of the ICM wave vector [24]; 3) a double-peak structure at low energy in optical conductivity due to the absorption of the electromagnons with a selection rule of the electric field along the  $b$ -axis; 4) no new peak splitting in the electromagnon spectra in the presence of external magnetic field along the  $a$ - or  $b$ -axis, which differs from the conventional picture of the Zeeman energy splitting of magnons; 5) the increase (decrease) of the energy gaps of the electromagnons as the field increases along the  $b(a)$ -axis.

**Magnetoelectric coupling.** – The ferroelectricity in  $\text{RMn}_2\text{O}_5$  is substantially different from that in  $\text{RMnO}_3$ . Experiments have shown that the ferroelectricity only exists along the  $b$ -axis in  $\text{RMn}_2\text{O}_5$ , but can be observed in both the  $a$  and  $c$  directions in  $\text{RMnO}_3$ . Most importantly, recent measurements of optical conductivity have revealed opposite selection rules for these two materials. In  $\text{RMnO}_3$ , low energy absorption is observed when the electric field is perpendicular to the static ferroelectric polarization direction [20,25]. The opposite is true in  $\text{RMn}_2\text{O}_5$ , namely, low energy absorption is only observed when the electric field is polarized along the  $b$ -axis [20]. This suggests that the electric degree of freedoms along the  $a$ - and  $c$ -axis simply has no coupling to magnetic degrees of freedom at low energy. Only the ferroelectricity along the  $b$ -axis  $P_b$  couples to the magnetic degree of freedom. The order parameter  $P_b$  is an Ising-type order. Therefore, the nature of the magnetoelectric coupling in  $\text{RMn}_2\text{O}_5$  is a coupling between two Ising-type orders. (In the following paper, we refer to the  $a$ -,  $b$ -,  $c$ -axis as the  $x$ -,  $y$ -,  $z$ -axis, respectively, for convenience *i.e.*  $P_y = P_b$ .)

What is the Ising order on the magnetic side? The answer to this question can be obtained by in-depth analysis of the magnetic structure and the space group. As shown in [17,18], the main magnetic structure along the  $a$ -axis is two antiferromagnetic chains joined by  $\text{Mn}^{3+}$  and  $\text{Mn}^{4+}$  atoms (see fig. 1). The antiferromagnetic coupling between the two chains indicated by the red lines in fig. 1 is completely frustrated. Therefore, in an effective model, we at least need two antiferromagnetic orders  $\vec{n}_1$  and  $\vec{n}_2$  to describe the magnetic physics. A possible Ising order from these two vector magnetic orders is  $\vec{n}_1 \cdot \vec{n}_2$ . Due to the experimental fact that no magnetic moment in the  $c$ -axis

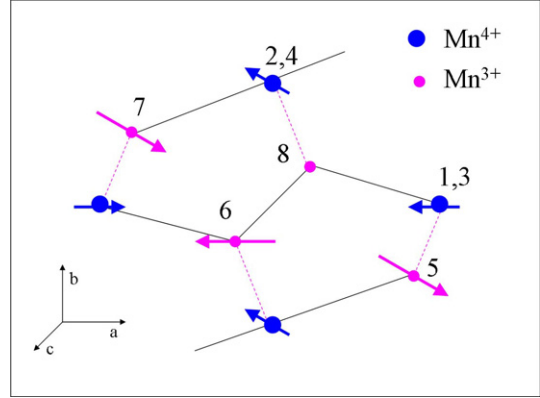


Fig. 1: (Colour on-line) A sketch of spin structures from a top view along the  $c$ -axis in one unit cell of  $\text{RMn}_2\text{O}_5$ . The red lines reflect the frustrated magnetic coupling between two chains.

is observed, this naturally leads to the construction of the possible lowest-order magnetoelectric coupling between  $P_y$  and  $\vec{n}_i$ ,  $i = 1, 2$  as

$$H_{em} = \lambda_x P_y n_1^x n_2^x + \lambda_y P_y n_1^y n_2^y. \quad (1)$$

The possible differences between the coupling parameters  $\lambda_x$  and  $\lambda_y$  reflects real lattice structure.

Now we show that eq. (1) is consistent with the space group analysis. The space group of  $\text{RMn}_2\text{O}_5$  has been analyzed in [26]. The lattice of  $\text{RMn}_2\text{O}_5$  belongs to  $Pbam$  structure. With the modulation vector  $q = (1/2, 0, k_c)$ , the space group has a single two-dimensional irreducible representation in which the four symmetry lattice transforms can be represented by  $I$ ,  $m_x = \sigma_x$ ,  $m_y = \sigma_y$ ,  $m_x m_y = i\sigma_z$ , where  $\sigma_i$  are Pauli matrices. Symmetry-adapted variables can be constructed as linear combinations of spin operators that transform in accordance with these matrices. The ion spins in one unit cell are numbered from one to eight as shown in fig. 1. The space inversion symmetry, together with the experimental facts that  $S_1 = S_3$ ,  $S_2 = S_4$ ,  $S_5 = S_7$ ,  $S_6 = -S_8$  and that the spin moments are only in the  $ab$ -plane, suggests that the possibilities of the magnetoelectric coupling term can be narrowed down to

$$\begin{aligned}
 H_{em} = & i\lambda_x P_y (-S_2^x(q) S_6^{x*}(q) + S_1^x(q) S_5^{x*}(q) - \text{c.c.}) \\
 & + i\lambda_y P_y (-S_2^y(q) S_6^{y*}(q) + S_1^y(q) S_5^{y*}(q) - \text{c.c.}) \quad (2)
 \end{aligned}$$

Converting these spin operators to the two antiferromagnetic orders, we can simplify eq. (2) to eq. (1).

While it is easy to understand the time-reversal invariance in eq. (1), the parity invariance is not manifest. Physically, this result comes from the antiferromagnetic order along the  $a$ -axis. We can understand it by examining fig. 1. By picking any pink bond, for example,  $S_1 - S_5$ , we see that after space inversion,  $S_5$  will become  $S_7$  and  $S_1$  will become  $S_3$  ( $S_3$  in the neighbor unit cell). From the antiferromagnetic structure,  $S_5 = S_7$  and  $S_1 = -S_3$ , therefore  $\vec{n}_1 \cdot \vec{n}_2$  changes sign under parity transformation, *i.e.*, if we call the antiferromagnetic order in the chain including

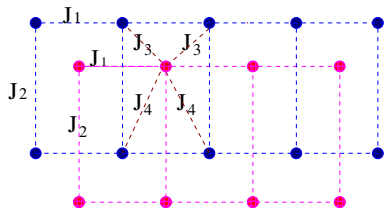


Fig. 2: (Colour on-line) A sketch of lattice structures of two frustrated coupled antiferromagnetic Heisenberg models in two dimension.

$S_1$  as  $\vec{n}_1$  and that in the chain including  $S_5$  as  $\vec{n}_2$ , under the parity transformation,  $\vec{n}_1$  goes to  $-\vec{n}_1$  and  $\vec{n}_2$  goes to  $\vec{n}_2$ .

**Effective magnetic model.** – In condensed-matter physics, an effective model at low energy is largely independent of microscopic models if they share the same essential physics. Therefore, one can derive the effective model on a much simplified lattice structure. In the case of  $\text{RMn}_2\text{O}_5$ , the important magnetic physics along the  $a$ -axis are two antiferromagnetic chains with frustrated coupling [17,18]. Experiments have shown a  $1/4$  commensurate magnetic wave vector along the  $c$ -axis, which can also be viewed as an antiferromagnetic order if the unit cell is doubled along the  $c$ -axis. Therefore, we can derive the effective model from a microscopic model with two antiferromagnetic orders defined on the two interpenetrating sublattices as illustrated in fig. 2, where  $J_{1,(2)}$  are the effective antiferromagnetic exchange couplings which establish two antiferromagnetic orders,  $J_3$  is the effective frustrated coupling between two chains in one unit cell along the  $a$ -axis and  $J_4$  is the effective frustrated coupling between two chains in two neighbor unit cells along the  $c$ -axis. Using the standard field theory [23,27], we can show that the effective field theory described by the two antiferromagnetic orders  $\vec{n}_1$  and  $\vec{n}_2$  is given by the following Hamiltonian:

$$H_m = \int \left\{ \sum_i \left[ \frac{\rho_{1s}}{2} \left( \frac{\partial n_i}{\partial x} \right)^2 + \frac{\rho_{2s}}{2} \left( \frac{\partial n_i}{\partial z} \right)^2 \right] + \alpha \left( n_1 \frac{\partial n_2}{\partial x} - n_2 \frac{\partial n_1}{\partial x} \right) - \tilde{g}(T)(n_1 \cdot n_2)^2 - D_0 \sum_i (n_i^x)^2 \right\} dx dz. \quad (3)$$

where  $\tilde{g}(T) = \tilde{g}_0 + \tilde{g}_1 T$  is a temperature-dependent parameter induced by the quantum and thermal fluctuation, the parameter  $\alpha$  reflects that the intra-frustrated coupling in one unit cell is larger than the inter-frustrated coupling along the  $a$ -axis between two neighbor unit cells along the  $c$ -axis, and the parameter  $D_0$  describes a possible magnetic easy axis along the  $a$ -axis. From the microscopic coupling parameter,  $\tilde{g}_1 = 0.26(J_1 + J_2)S a^{-2} \left( \frac{J_3 + J_4}{J_1 + J_2} \right)^2$ ,  $\tilde{g}_2 = 2.4 \frac{\tilde{g}_1}{(J_1 + J_2)S}$ ,  $\rho_{1s} = J_1 S^2$ ,  $\rho_{2s} = J_2 S^2$ ,  $\alpha = \frac{(J_1 + J_2)S^2}{4} \frac{(J_3 - J_4)}{(J_1 + J_2)a}$ . Adding the lattice dynamics, we reach the total effective Hamiltonian as

$$H = \int dx dz \left[ \left( \frac{\kappa}{2} P_y^2 + \frac{1}{2M} \pi_y^2 \right) + H_{em} \right] + H_m, \quad (4)$$

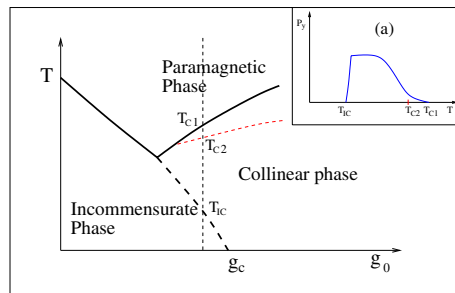


Fig. 3: (Colour on-line) The phase diagram as  $g_0$  vs.  $T$ . The vertical dashed line represents phase transitions in most of  $\text{RMn}_2\text{O}_5$  materials. The inset (a) is the ferroelectricity as a function of temperature.

where  $\pi_y$  is the conjugate momentum of  $P_y$ . The Hamiltonian in eq. (4) precisely captures the phase diagrams of  $\text{RMn}_2\text{O}_5$  [4,15,16]. To study the magnetic phase diagram, we can integrate out the lattice dynamics. After integrating out the lattice dynamics, the effective magnetic Hamiltonian is the Hamiltonian in eq. (3) with a replacement of  $\tilde{g}$  by  $g(T) = g_0 + \tilde{g}_1 T$ , where  $g_0 = \tilde{g}_0 + \frac{\lambda_{\pm}^2}{8\kappa}$ ,  $D_0$  by  $D = D_0 + \frac{\lambda_+ \lambda_-}{4\kappa}$  and an additional term  $-\gamma(n_1^x n_2^x - n_1^y n_2^y)^2$  where  $\gamma = \frac{\lambda_{\pm}^2}{8\kappa}$  and  $\lambda_{\pm} = \lambda_x \pm \lambda_y$ . It is clear that the  $\alpha$ -term favors an ICM phase, while  $g(T)$ ,  $\gamma$  and  $D$  favor a CM phase. If  $D \neq 0$ , at relatively high transition temperature  $T_{c1}$ , the model exhibits a first phase transition to a collinear magnetic phase with order  $\langle n_1^x n_2^x \rangle \neq 0$  and then exhibits a second phase transition at  $T_{c2} < T_{c1}$  with order  $\langle n_1^y n_2^y \rangle \neq 0$ . The ferroelectricity is given by  $\langle P_y \rangle = -\frac{\lambda_x \langle n_1^x n_2^x \rangle + \lambda_y \langle n_1^y n_2^y \rangle}{\kappa}$ . With the proper values of  $\alpha$ , at a low temperature  $T_{IC}$ , the ICM phase can win over the commensurate magnetic phase. In the ICM phase, the global average,  $\langle P_y \rangle = 0$ . Figure 3 sketches the phase diagram. The phase diagram qualitatively matches the current experimental results on the phase diagram of  $\text{RMn}_2\text{O}_5$  [4,15,16]. Results from mean-field or large- $N$  limit calculation, using the real experimental data as input, will be reported elsewhere [28].

In the following, we calculate the low-energy excitations from this model and we show that it matches experimental results very well. We assume  $\rho_{1s} = \rho_{2s} = \rho$  for simplifying our calculation. The dispersion of low-energy excitations along the  $z$ -direction has a simple form,  $\rho k_z^2$ , regardless of the ground states. Therefore, we only need to calculate the dependence of the dispersion on  $k_x$ .

### Energy dispersion of magnons in the CM phase.

– In the CM phase, the ferroelectricity,  $\langle P_y \rangle = -\frac{\lambda_+ + \lambda_-}{2\kappa}$ . The dynamics of magnons and the dynamics of electric degree of freedoms are decoupled. To show this, one can expand the free energy in the vicinity of the ground state and show that there is no second-order coupling between the lattice and magnetic dynamics. Therefore, there is no electromagnon excitation. The energy dispersions of the

two magnons in the CM phase are given by

$$E_{cm}^{\pm}(k_x) = \sqrt{\rho(\rho k_x^2 + \gamma + g + D \pm \sqrt{(g - \gamma)^2 + \alpha^2 k_x^2})}. \quad (5)$$

**Electromagnons in the ICM phase.** – In the ICM phase,  $\langle P_y(x) \rangle = -\frac{\lambda_{\pm}}{2\kappa} \cos(qx)$ , where  $q$  is the ICM wave vector. The magnon and phonon dynamics are coupled due to the ICM modulation. Therefore, the low-energy excitations are electromagnons. To calculate the dispersion, we expand the Hamiltonian in the vicinity of the ICM phase and let  $u_1, u_2$  and  $\beta$  be the deviations of the first, second magnetic orders and lattice position from the mean-field solution, respectively. The fluctuation up to the second order of these dynamic variables is given by  $\delta H^{(2)} = \delta H_0^{(2)} + \delta H_1^{(2)}$ . The first term is the free part given by

$$\delta H_0^{(2)} = \sum_{k_x} \left( \sum_{i=1}^2 E_i(k_x) \mu_i(k_x) \mu_i(-k_x) + \omega_0^2 \beta(k_x) \beta(-k_x) \right) \quad (6)$$

with  $E_1(k_x) = \rho k_x^2 + \frac{D a_1}{2} + \frac{\lambda_-(a_1 \lambda_+ + \lambda_-)}{4\kappa}$ ,  $E_2(k_x) = E_1(k_x) + \Delta_0$ , where  $\Delta_0 = \alpha q - 2\tilde{g} - \frac{\lambda_-^2}{4\kappa}$  and the phonon frequency  $\omega_0 = \sqrt{\kappa}$  (for convenience, we have taken the mass  $M = 1$  in eq. (4)). The second term is the interaction part

$$\delta H_1^{(2)} = \int dx \left[ \alpha a_1 \cos(qx) u_1' u_2 + D \sin(qx) u_1 u_2 + \frac{1}{2} \beta (-\lambda_- u_1 \sin(qx) + \lambda_+ u_2) \right]. \quad (7)$$

In eq. (7), the terms on the first line couple  $u_1(k_x)$  with  $u_2(k_x \pm q)$  and vice versa and modify the gap  $\Delta_0$  between two magnon modes. In general, as shown in fig. 4, the coupling creates a distinguished kink in the dispersion curve around  $k_x = q/2$  rather than a finite energy jump at  $k_x = q/2$  which is normally expected in the ICM phase described in a simple Sine-Gordon model [24]. The terms on the second line describe the coupling between the magnon and the phonon. The coupling results in two general effects. First, the coupling leads to a change of phonon frequency. Under the condition  $\omega_0^2 \gg \rho E_i(0)$ , the shift frequency of the phonon is roughly given by  $\delta\omega^2 = \frac{\rho\lambda_+^2}{4(\omega_0^2 - \rho E_2(0))} + \frac{\rho\lambda_-^2}{8(\omega_0^2 - \rho E_2(q))}$ . Second, the coupling allows us to measure the magnons in optical conductivity. The optical conductivity is given by  $\sigma(\omega) = \omega \text{Im}[G_{\beta\beta}(\omega, 0)]$ , where  $G_{\beta\beta}(\omega, k_x)$  is the full propagator of the  $\beta$ . In our model, we expect double peaks in the optical conductivity at the gap energy of the two magnons in the ICM phase. Up to the second order, we have,  $\text{Im}[G_{\beta\beta}(\omega, 0)] = \pi \left[ \rho \frac{\lambda_-^2}{8\omega_0^4} \delta(\omega^2 - \rho E_1(q)) + \rho \frac{\lambda_+^2}{4\omega_0^4} \delta(\omega^2 - \rho E_2(0)) + (1 - \rho \frac{\lambda_-^2/2 + \lambda_+^2}{4\omega_0^4}) \delta(\omega^2 - \omega_0^2 - \delta\omega^2) \right]$ . In fig. 4, by numerically solving the dynamical equations of  $\delta H^{(2)}$ ,

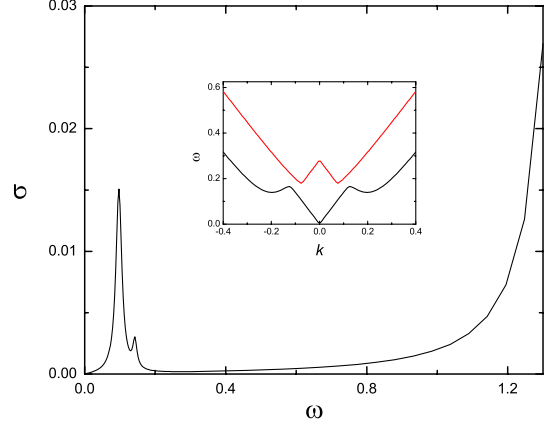


Fig. 4: (Colour on-line) The numerical result of the optical conductivity vs. frequency with the parameters set to  $\{\rho, \alpha, \lambda_+, \lambda_-, \kappa, D, g\} = \{2, 0.4, 0.06, 0.06, 2, 0.002, 0.005\}$ . The inset is the dispersion of the electromagnons.

we plot the result of  $\sigma(\omega)$  and the dispersions of electromagnons with a typical parameter setting  $\{\rho, \alpha, \lambda_+, \lambda_-, \kappa, D, g\} = \{2, 0.4, 0.06, 0.06, 2, 0.002, 0.005\}$ .

#### Quantitative comparison with experiments.

– The electromagnon has been detected in a recent paper [20]. From experiments, there are two important quantitative values. One is the energy of the electromagnon (the peak position) and the other is the intensity of the electromagnon peak. From our model, we predict two close-by electromagnon peaks whose positions are given by  $\omega_1 \sim \omega_2 \sim \rho\alpha/2$ , where  $\alpha = 2q$ . From experiments [4,12–16,18],  $q \approx 0.12$ , which implies  $\alpha \approx 0.24$ . For the peak position at  $10 \text{ cm}^{-1}$  as shown in ref. [20],  $\rho \simeq 10 \text{ meV}$ , which is of a right order as far as its paramagnetic-antiferromagnetic transition temperature is concerned. From our model, the intensity of the electromagnon peak can also be calculated, which is given by  $I_{theory} = \frac{3\pi n e^{*2} \rho \lambda_{\pm}^2}{4\hbar^2 \kappa^2}$ . If we take  $\lambda_+ \sim \lambda_- \sim \lambda$ , and make use of  $P_y = n e^* (\lambda_+ + \lambda_-) / \kappa$ , we have  $\lambda = \kappa P_y / (2n e^*)$  where  $n$  is the volume of a lattice unit cell. We have

$$I_{theory} \sim \frac{3\pi \rho P_y^2}{16\hbar^2 n}. \quad (8)$$

Since all the variables can be measured or determined by the material itself, the result provides an independent check of our theory. Substituting the experimental values of  $n \sim 3.6 \times 10^{-3} \text{ \AA}^{-3}$  and  $P_y \sim 100 \mu\text{C}/\text{cm}^2$  and  $\rho \sim 10 \text{ meV}$ , we obtain  $I \sim 10^{14} \Omega^{-1} \text{ m}^{-1} \text{ s}^{-1}$ , a number that is in a good agreement with the experimental result,  $4 \times 10^{13} \Omega^{-1} \text{ m}^{-1} \text{ s}^{-1}$ , considering the complicated nature of materials. Finally, given that  $\kappa \sim 1 \text{ eV}/\text{\AA}^2$  and  $e^* \sim 10e$  [8], we can estimate the order of the magnetoelectric coupling constant to be of the order of  $1 \text{ meV}$ .

**Effects of external magnetic field.** – In our model, since  $\vec{n}$  is the staggered moment field, the effect of an

external magnetic field  $H$  is equivalent to creating an easy plane. However, since the staggered moment is in the  $ab$ -plane, the effect of the field is only important when the field is along the  $a$ - or  $b$ -axis. In the presence of the easy-axis parameter  $D$  along the  $a$ -axis, the effects of the external magnetic fields along the  $a$ -axis,  $H_a$ , and  $b$ -axis,  $H_b$ , have exact opposite effects. They simply change  $D$  to

$$D(H_a, H_b) = D - H_a^2/2\rho + H_b^2/2\rho. \quad (9)$$

From  $E_1(k)$ ,  $E_2(k)$ , eq. (7) and eq. (9) lead to a few important and immediate predictions. First, the effects of  $H_a$  and  $H_b$  do not depend on their directions along their own axis. Second,  $H_b$  can drive the system from the ICM phase to the CM phase, while  $H_a$  can drive the system from the CM phase to the ICM phase. This result has been observed experimentally in [12]. Third, in the ICM phase, the energy dispersions of the electromagnons as a function of  $H_a$  and  $H_b$  can be predicted. From  $E_1(k)$ ,  $E_2(k)$  and eq. (7), the energy of the electromagnons is expected to increase (decrease) as  $H_b$  ( $H_a$ ) increases. Finally, the external magnetic field does not add additional peaks, which contradicts the conventional picture of the Zeeman energy splitting of magnons.

In conclusion, we develop an effective model that explains the phase diagram and the mechanism of magnetoelectric coupling in multiferroics  $\text{RMn}_2\text{O}_5$ . To our knowledge, this is the first theoretical effective model for these materials. A detailed study of low-energy excitations is performed to explain the selection rules of electromagnons in optical conductivity measurements [20]. Our theory not only quantitatively matches experimental results of the energy and intensity of electromagnons but also predicts the electromagnon dispersion and its dependence on the external magnetic field that can be tested in future experiments.

There is a fundamental difference of the magnetic structures between  $\text{RMn}_2\text{O}_5$  and  $\text{RMnO}_3$ . The magnetic structure in  $\text{RMn}_2\text{O}_5$  requires two independent antiferromagnetic order parameters in one unit cell due to the complexity of its unit cell, while a single magnetic order parameter sufficiently describes the magnetic structure in  $\text{RMnO}_3$ . This fundamental difference shows the possibility of different effective theories in these two different materials. We expect that the model presented here can be applied to other multiferronics materials where ferroelectricity is correlated to a collinear magnetic phase.

\*\*\*

JH thanks S. KIVELSON and S. BROWN for teaching some concepts presented in this paper. We thank A. B. SUSHKOV, R. V. AGUILAR and D. DREW for important comments and extremely useful discussions. We also thank M. MOSTOVOY for useful discussions at the APS March meeting (2007). This work was supported

by the National Science Foundation under grant No. PHY-0603759.

## REFERENCES

- [1] TOKURA Y., *Science*, **312** (2006) 1481.
- [2] CHEONG S. W. and MOSTOVOY M., *Nat. Mater.*, **6** (2007) 13.
- [3] KIMURA T., GOTO T., SHINTANI H., ISHIZAKA K., ARIMA T. and TOKURA Y., *Nature*, **426** (2003) 55.
- [4] HUR N., PARK S., SHARMA P. A., AHN J. S., GUHA S. and CHEONG S. W., *Nature*, **429** (2004) 392.
- [5] KIMURA T., KAWAMOTO S., YAMADA I., AZUMA M., TAKANO M. and TOKURA Y., *Phys. Rev. B*, **67** (2003) 180401.
- [6] GOTO T., KIMURA T., LAWES G., RAMIREZ A. P. and TOKURA Y., *Phys. Rev. Lett.*, **92** (2004) 257201.
- [7] MOSTOVOY M., *Phys. Rev. Lett.*, **96** (2006) 067601.
- [8] KATSURA H., NAGAOSA N. and BALATSKY A. V., *Phys. Rev. Lett.*, **95** (2005) 057205.
- [9] KATSURA H., BALATSKY A. V. and NAGAOSA N., *Phys. Rev. Lett.*, **98** (2007) 027203.
- [10] SERGIENKO I. A. and DAGOTTO E., *Phys. Rev. B*, **73** (2006) 094434.
- [11] HU J., *Phys. Rev. Lett.*, **100** (2008) 077202.
- [12] HUR N., PARK S., SHARMA P. A., GUHA S. and CHEONG S. W., *Phys. Rev. Lett.*, **93** (2004) 107207.
- [13] CHAPON L. C., BLAKE G. R., GUTMANN M. J., PARK S., HUR N., RADAELLI P. G. and CHEONG S. W., *Phys. Rev. Lett.*, **93** (2004) 177402.
- [14] KADOMTSEVA A. M., KROTOV S. S., POPOV Y. F. and VOROB'EV G. P., *Low Temp. Phys.*, **32** (2006) 709.
- [15] KIGOMIYA I., MATSUMOTO S., KOHN K., FUKUDA Y., SHOBU T., KIMURA H., NODA Y. and IKEDA N., *Ferroelectrics*, **286** (2003) 167.
- [16] CHAPON L. C., BLAKE G. R., GUTMANN M. J., PARK S., HUR N., RADAELLI P. G. and CHEONG S.-W., *Phys. Rev. Lett.*, **93** (2004) 177402.
- [17] CHAPON L. C., RADAELLI P. G., BLAKE G. R., PARK S. and CHEONG S.-W., *Phys. Rev. Lett.*, **96** (2006) 097601.
- [18] BLAKE G. R., CHAPON L. C., RADAELLI P. G., PARK S., HUR N., CHEONG S.-W. and RODRIGUEZ-CARVAJAL J., *Phys. Rev. B*, **71** (2005) 214402.
- [19] RADULOV I., LOVCHINOV V. and DASZKIEWICZ M., *cond-mat/0701687* (2007).
- [20] SUSHKOV A. B., AGUILAR R. V., PARK S., CHEONG S.-W. and DREW H. D., *Phys. Rev. Lett.*, **98** (2007) 027202.
- [21] SHENDER E. F., *Sov. Phys. JETP*, **56** (1982) 178.
- [22] CHANDRA A. L. P. and COLEMAN P., *Phys. Rev. Lett.*, **64** (1990) 88.
- [23] HENLEY C. L., *Phys. Rev. Lett.*, **62** (1989) 2056.
- [24] BAK P., *Rep. Prog. Phys.*, **45** (1982) 587.
- [25] PIMENOV A., MUKHIN A. A., IVANOV V. Y., TRAVKIN V. D., BALBASHOV A. M. and LOIDL A., *Nat. Phys.*, **2** (2006) 97.
- [26] HARRIS A. B., *cond-mat/0610241* (2006).
- [27] TSVELIK A. M., *Quantum Field Theory in Condensed Matter Physics* (Cambridge University Press) 2003.
- [28] FANG C. and HU J., in preparation.